Astron. Astrophys. 357, 1020–1030 (2000)

ASTRONOMY AND ASTROPHYSICS

The NGC 6334 IV massive star formation site: a cluster in the making?⋆

P. Persi[1], **M. Tapia**[2], **and M. Roth**[3]

[1] Istituto Astrofisica Spaziale, CNR, Area di Ricerca Tor Vergata, Via del Fosso del Cavaliere, 00133 Roma, Italy (persi@saturn.ias.rm.cnr.it)
[2] Instituto de Astronomia, UNAM, Apartado Postal 877, Ensenada, Baja California, CP 22830, Mexico
[3] Las Campanas Observatory, Carnegie Institution of Washington, Casilla 601, La Serena, Chile

Received 24 November 1999 / Accepted 17 February 2000

Abstract. Sub-arcsecond JHK images of the star formation region NGC 6334 IV covering 14.7 sq arcmin have been obtained. These were supplemented by H_2 and Brγ images of the central 2 sq arcmin. A total of 1238 sources brighter than $K \simeq 17$ were detected. Due to the very high extinction in this region, only 685 of these are brighter at 1.2 μm than our limit, $J \simeq 20$. Only less than 5% of the sources exhibit excess emission at $\lambda > 2.0\,\mu$m and they are scattered over the whole area covered. No evidence of a developed stellar cluster was found, but a small number of luminous (O–B2) young stellar objects were detected. These are embedded in the densest part of the molecular cloud that is at the centre of a giant bipolar structure seen in the radio and the infrared. This morphology is the result of the effect of massive stellar winds originating from the centre of a dense molecular toroid which collimates the outflow material giving rise to two lobes of thermal gas and dust emission. We confirm that the extinction is higher toward the southern lobe than toward the northen one but both are less reddened than their immediate surroundings. A new centre of active massive star formation is reported to the east of the central region. Close to a (sub)millimeter emission peak, a large infrared nebula with several point-like sources was found at 2.2 μm. The discovery of a small embedded low-luminosity bipolar object in the vicinity of one of the giant lobes is also reported.

Key words: stars: formation – ISM: clouds – ISM: dust, extinction – ISM: H II regions – infrared: stars

1. Introduction

The molecular cloud complex NGC 6334 is proving to be a challenge to our understanding of high mass star formation processes since no single model or theoretical scenario can explain the combined characteristics of even any two centres of activity in this huge complex.

Emerson et al. (1973) discovered a chain of five equally separated bright far-infrared peaks (McBreen et al. 1979; Loughran et al. 1986), all associated with catalogued radio HII regions and OH masers and immersed within or very close to the large optical nebula NGC 6334. We now know that it consists of several centres or spots of active star formation, occurring in a single collapsing molecular cloud (Dickel et al. 1977) at a distance of 1.7 kpc, as determined for the several O-type visible stars associated with it (Neckel 1978). NGC 6334 has subsequently been observed in greater detail at several wavelengths, ranging from the optical –photometry and spectroscopy of OB-type stars and associated nebulae– to the radio –continuum and atomic and molecular line emission– and practically all available wavelength windows in-between.

In the *early days*, simplistic scenarios were proposed to explain the large-scale characteristics of all the star forming centres in the region (Dickel et al. 1977; Rodríguez et al. 1982), but with deeper and more detailed observations, the picture now appears more complex. For example, in the vicinity of NGC 6334 I (for an explanation of the current nomenclature of the objects in this region see the Appendix in Kraemer et al. 1999), there are in an area of less that 2 sq pc, at least two separate collimated massive outflows and a developed and a compact HII region, the last with a multiple, very young stellar system immersed. There is also an embedded stellar cluster composed of medium (and presumably also low) mass stars. The ages and masses derived for each of these objects vary amply, indicating a clear non-coeval star formation process (with time-scales of up to a few million years) in spatial scales of one or two parsec and, quite importantly, with no apparent geographical correlation whatsoever (Persi et al. 1996; Tapia et al. 1996).

NGC 6334 IV is characterized by the presence of two extended low emissivity lobes detected in radio (Rodríguez et al. 1988) and infrared wavelengths (Harvey et al. 1987; Kraemer et al. 1999). Near their midpoint, two bright mid-infrared sources are located, one of them (IRS-IV-2; Harvey & Gatley 1983) coincides with a bright shell radio HII region, known as NGC 6334 A, and the second is a bright and extended source (IRS-IV-3) with a much fainter radio continuum emission. Recent high-resolution 12.5 and 21 μm maps by Kraemer et al. (1999) have shown that these sources are also extended and

Send offprint requests to: P. Persi

⋆ The complete list of the detected sources including their positions and photometry is available in electronic form at the CDS

Correspondence to: Istituto Astrofisica Spaziale, CNR, Area di Ricerca Tor Vergata, Via del Fosso del Cavaliere, 00133, Roma, Italy

multiple. Several NH_3 clumps (Kraemer et al. 1997) and one H_2O maser (Rodríguez et al. 1980) are also located very close to these sources. All these constitute a small, multiple system of massive stars being or just being formed at the centre of a dense molecular structure, possibly a rotating disk (Kraemer et al. 1997). These immersed young objects provide a large fraction of the ionizing, thermal and kinematic energy to the gas and dust in the lobes (Rodríguez et al. 1988, De Pree et al. 1995).

In the present work, we present a detailed near-infrared study of an area 230×230 sq arc sec centred on NGC 6334 IV. This is based on JHK mosaiced images supplemented by H_2+continuum and Brγ+continuum frames of the central part. The observations, reduction and photometric results are described in the next section and the derived overall properties are discussed in Sect. 3 together with a discussion of the individual set of objects. Finally, the last section summarizes the new findings.

2. Observations and results

We obtained one mosaic of 5×5 overlapping frames covering an area of 230×230 sq arc sec centred at $\alpha(1950) = 17^{\rm h}16^{\rm m}56.7^{\rm s}$ $\delta(1950) = -35^o51'58''$ in each of the J, H and K bands. Additionally, the central 85×85 sq arcsec was also imaged through the narrow-band filters: $\lambda_o = 2.125\,\mu$m, $\Delta\lambda = 0.024\,\mu$m, which includes the $2.12\,\mu$m molecular hydrogen $\nu = 1 \rightarrow 0$ S(1) line; and $\lambda_o = 2.20\,\mu$m, $\Delta\lambda = 0.11\,\mu$m, which includes the Br$\gamma$ line and continuum. The exposure times were 360 s and 240 s for the H_2 and Brγ filters, respectively, and 480 s, 300 s and 100 s for the JHK frames. A set of standard stars were also observed each night to provide photometric calibrations.

The observations were made with the IR camera (Persson et al. 1992) attached to the 2.5m DuPont telescope at Las Campanas Observatory the nights of 1997 May 19–22. The image scale was $0.35''$ per pixel and the mean point-spread function (FWHM) was less than $1''$.

Star positions were determined using a grid of stars included in the HST Guide Star Catalogue. We estimate that all positions reported in this work are accurate to less than $1''$. Stellar photometry was performed using the DAOPHOT package (Stetson 1987) within the IRAF environment with an aperture of $2''$. The point-spread function for each frame was derived for several isolated stars to be used in the photometric procedure using the ALLSTAR option. Zero points were calculated from the standard stars in use at Las Campanas. These were observed before and after the object at similar airmasses and were reduced in a similar way as the program stars. The results of the gaussian fits from ALLSTAR were adopted for our photometry in order to avoid larger uncertainties due to possible small fluctuations in the background introduced when the mosaics were constructed from the individual pre-reduced frames. After considering all different sources of error such as psf and aperture corrections, zero-point and background fluctuations, and the small deviations due to airmass differences, we estimate the accuracy of our photometry to be $\sim$ 0.1–0.15 mag (except for the faintest sources).

We detected 1238 sources in the K band, 993 in H and 685 in J, with estimated completeness limits (see below) of 16.2 at K, 17.8 at H and 18.3 at J. The drastic drop in the number of sources detected at the shorter wavelengths in spite of greater sensitivity gives the first clue of the extremely high interstellar extinction affecting the light from the stars. As will be discussed in the next section, most of the dust extinction is caused by material associated with NGC 6334.

With two exceptions, explained by confusion effects, all sources detected by Harvey et al. (1987)(HHS) were also recorded in the present survey. Due to the high density of sources and the highly variable diffuse emission in the region, no reliable quantitative comparisons can be made between our imaging psf photometry and the aperture ($3.5''$) single-detector photometry by HHS. For point sources in common that were brighter than $K = 12.5$, $\langle \Delta K \rangle_{\rm (ours-HHS)} = 0.06 \pm 0.04$ (sd) while these differences and scatter increase significantly for fainter source magnitudes, as expected in the presence of extended emission or fainter sources included in HHS's beam. We notice, however, a systematic error in the declination given by Harvey et al. (1987). The mean differences between the coordinates derived for this work *minus* those reported by HHS are: $\langle \alpha \rangle = 0.004^{\rm s}$ (s.d. = 0.03) and $\langle \delta \rangle = 2.8''$ (s.d. = 0.09). These systematic AAT coordinate shifts have already been reported by Tapia et al. (1996) with reference to Straw et al. (1989) work on the nearby NGC 6334 I.

The combined pseudoreal colour (J represented in blue, H in green and K in red) image is presented in Fig. 1, while Fig. 2 shows the narrow-band filter images centred at H_2 (2.125 μm) and at 2.20 μm, which includes the Brγ line. From the comparison of these two images we exclude the presence of molecular hydrogen emission in the central part of NGC 6334 IV, but a bright spot of emission in the Brγ hydrogen recombination line in the north lobe is evident.

3. Discussion

3.1. Colour-colour and colour-magnitude diagrams

The $J - H$ vs $H - K$ diagram of the 682 sources detected in the three passbands is reported in Fig. 3. We note that most of the infrared sources are aligned along the reddening line forming a band of width determined by the photometric errors. Only approximately 5% of the sources show significant infrared excesses, i.e. sources with $H - K$ indices deviating more than 0.15 to the right of the early-type-photosphere reddening line on the two-colour diagram (Fig. 3). The location of a few objects to the left of the reddening line for late-type stars is caused by unusually large photometric errors. The list of those sources with near-IR excess, their coordinates, JHK photometry and intrinsic errors are given in Table 1.

Further information about the nature of the sources detected can be extracted from the colour-magnitude K vs $H - K$ plot (Fig. 4). All sources observed in JHK, plus some 200 stars fainter than our limit at 1.2 μm but still above the detection

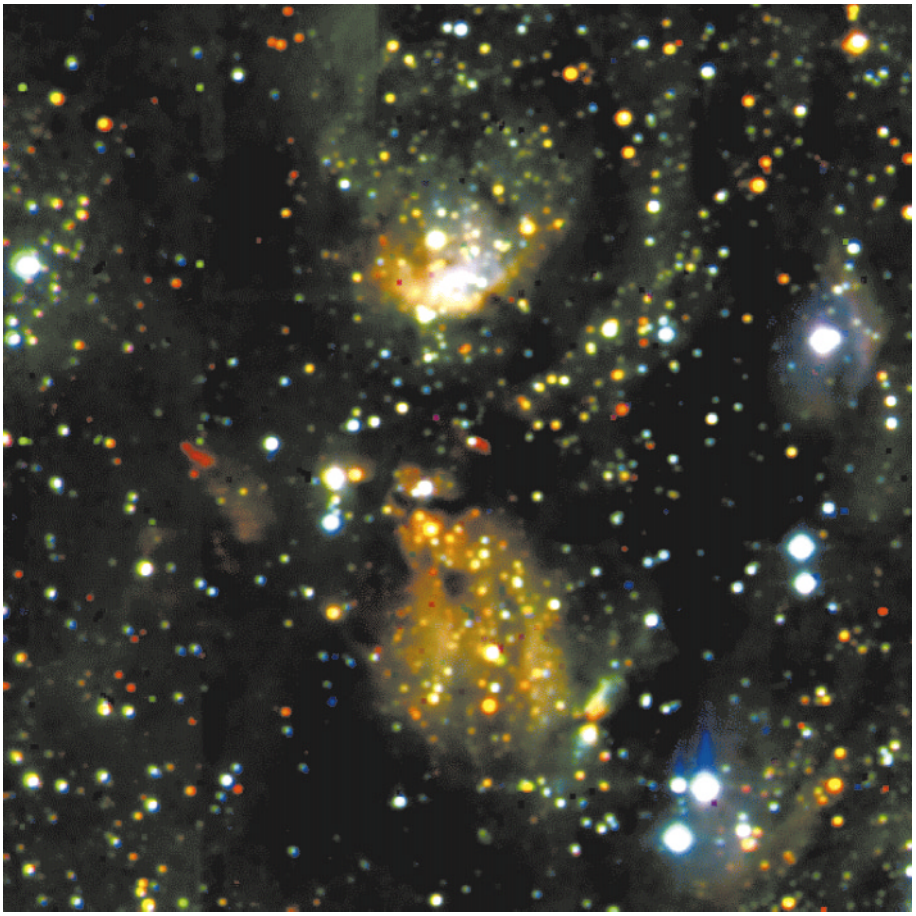

Fig. 1. *True color* image of NGC 6334 IV made from the J (blue), H (green) and K individual images covering 230×230 sq arcsec. North is to the top, east to the left

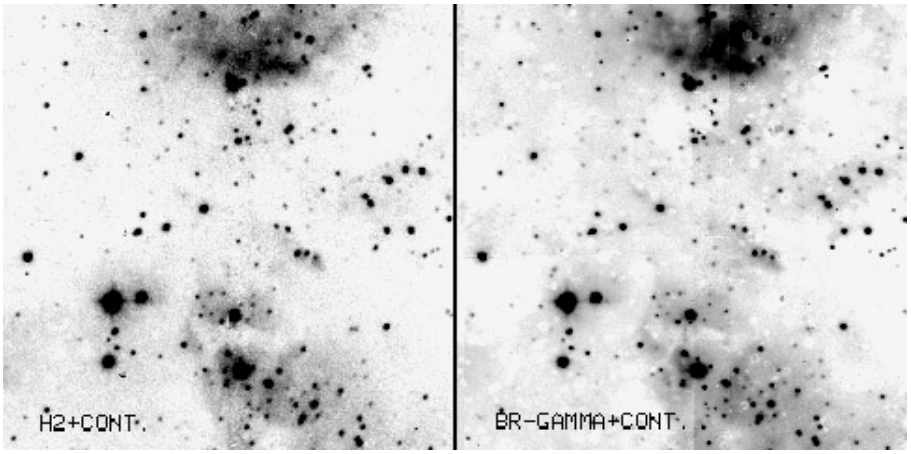

Fig. 2. Narrow band images at 2.125 μm and 2.20 μm of the central area (85×85 sq arcsec) of NGC 6334 IV

threshold in H and K are plotted. According to the discussion presented by Tapia et al. (1996) for NGC 6334 I, sources fainter than $K = 13.5$ and with $H - K \leq 0.75$ are foreground field stars; sources detected only in H with K brighter than 15 with $H - K \geq 2$ are reddened stars earlier than B3-B5 embedded in the molecular cloud.

3.2. Stellar distribution

It is well established that the formation of high-mass stars is accompanied with the simultaneous or subsequent formation of a cluster of less massive stars. In very young complexes, the presence of these star clusters can only be determined and subsequently studied in the near-infrared as these objects are still deeply embedded in their parental cloud. In practically all known cases where O-B0 type stars have recently been formed, the presence of their lower mass counterparts forming a well defined cluster (see below) has been confirmed (eg. Lada & Lada 1991; Persi et al. 1994; Tapia et al. 1991, 1996, 1997).

A quick examination of the JHK images (Fig. 1) renders the impression that in NGC 6334 IV, embedded clusters may be associated with the northern and southern lobes almost symmet-

Table 1. List of the near-IR sources with IR excess.

No.	$\alpha(1950)$ h m s	$\delta(1950)$ ° ′ ″	K	$\sigma(K)$	H	$\sigma(H)$	J	$\sigma(J)$
1	17 16 49.15	-35 50 44.0	15.16	0.06	17.64	0.11	18.11	0.15
2	17 16 49.70	-35 53 11.8	15.87	0.07	17.34	0.05	18.01	0.04
3	17 16 50.03	-35 52 35.9	15.82	0.07	17.81	0.09	19.81	0.14
4	17 16 50.06	-35 50 46.8	15.95	0.08	17.61	0.09	19.36	0.15
5	17 16 50.91	-35 51 33.2	15.37	0.04	17.32	0.09	18.26	0.04
6	17 16 53.62	-35 53 13.1	13.28	0.03	15.39	0.03	16.86	0.03
7	17 16 55.21	-35 53 35.7	17.17	0.16	18.42	0.11	19.40	0.11
8	17 16 55.74	-35 52 20.1	14.84	0.05	16.44	0.08	17.74	0.03
9	17 16 56.25	-35 51 49.6	16.82	0.08	17.80	0.09	18.45	0.05
10	17 16 57.17	-35 51 17.2	15.08	0.13	16.27	0.12	16.97	0.16
11	17 16 57.72	-35 52 02.3	14.75	0.10	16.72	0.08	19.13	0.13
12	17 16 58.14	-35 51 43.9	15.78	0.09	17.11	0.04	17.91	0.05
13	17 17 00.20	-35 53 02.8	13.45	0.02	16.19	0.03	19.51	0.12
14	17 17 00.70	-35 50 35.0	16.96	0.12	18.22	0.09	18.93	0.09
15	17 17 02.15	-35 50 48.9	15.99	0.04	16.73	0.03	17.00	0.03
16	17 17 03.18	-35 53 48.4	12.88	0.04	14.74	0.01	16.77	0.05
17	17 17 03.44	-35 50 42.9	15.36	0.03	16.67	0.03	17.57	0.06
18	17 17 03.47	-35 51 32.1	14.21	0.05	15.63	0.04	16.85	0.04
19	17 17 03.71	-35 52 00.5	14.41	0.03	16.88	0.03	20.07	0.17
20	17 17 03.84	-35 52 58.1	16.05	0.06	18.00	0.07	19.97	0.15
21	17 17 03.92	-35 50 50.1	15.00	0.03	16.99	0.07	18.28	0.06
22	17 17 04.00	-35 52 45.6	16.00	0.07	17.46	0.05	18.95	0.08
23	17 17 04.46	-35 51 06.0	15.77	0.05	17.01	0.04	18.08	0.06
24	17 17 04.52	-35 52 36.0	17.59	0.17	18.42	0.10	18.89	0.08
25	17 17 04.99	-35 53 30.0	14.71	0.02	16.35	0.02	17.52	0.08
26	17 17 05.19	-35 53 50.5	14.93	0.04	15.98	0.03	16.77	0.03
27	17 17 05.55	-35 51 28.2	14.48	0.02	16.32	0.08	18.17	0.04
28	17 17 05.58	-35 53 00.5	15.91	0.04	17.55	0.08	18.11	0.05
29	17 17 05.64	-35 51 19.6	15.31	0.03	17.85	0.20	18.60	0.09
30	17 17 05.63	-35 52 01.6	15.32	0.05	17.26	0.06	17.84	0.05
31	17 17 05.74	-35 53 14.9	13.50	0.02	15.02	0.06	16.67	0.05
32	17 17 05.76	-35 53 31.4	15.68	0.05	17.80	0.09	19.03	0.08

rically placed relative to the young stellar objects HHS 19 (HG IRS 2) and HHS 20 (HG IRS 3). In fact, there is an apparent concentration of stars in these zones as seen in Fig. 5 (upper left panel), where all detected (in K) stars are plotted. The following analyses will demonstrate that such enhanced concentrations of near-infrared sources are the result of lower dust column densities toward those areas and that no physical embedded cluster exists (note that by *cluster* we mean a physically associated conglomerate of stars of a wide range of masses roughly following a power law distribution).

First, we point out that, contrary to other embedded clusters of very young age, the fraction of stars showing excess emission at $\lambda > 2\,\mu$m, as determined by their position in the $H-K$ vs $J-H$ diagram (Fig. 3), is extremely low, amounting to some 5%, with a similar fraction of sources with colour index $H-K > 2$ and too faint to be detected in J, which may also have K-band excesses although for some this large index can be due to extremely large reddening. We then separate the population of stars in the sample (measured in all JHK bands) into two groups, those with near-IR excess and those with no excess; we add to the former, those measured at H and K only but with $H-K > 2$, and study their spatial distribution. The upper right panel of Fig. 5 gives the spatial distribution of all stars with no IR excess, while the distributions for those with IR excess together with those with $H-K > 2$ and no J detection are shown in the lower left panel of Fig. 5. Finally, the lower right panel of the same figure shows stars only detected at K (and too faint at H and J).

The surprising result is that most of the stars with IR excess (reported in Table 1) expected to be members of the embedded stellar cluster are located well away from the *apparent* clusterings of stars, towards the SE in a region which we would consider representative of the field. These concentrations, however, are still clearly seen for the (normal) stars with no infrared excess. Additionally, the sample of stars detected only at K shows an almost random distribution, and their true characteristics would not alter the conclusion that no embedded young stellar cluster is associated with NGC 6334 IV.

What, then, causes the apparent stellar concentrations? In order to address this question, we have selected four separate areas within our studied region, each representative of the different expected stellar populations: Areas a and b are defined to

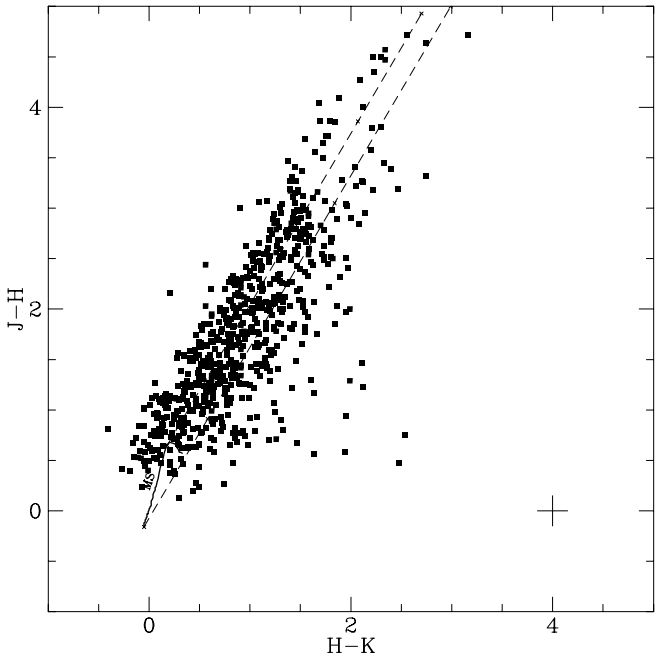

Fig. 3. $J-K$ vs $H-K$ diagram of 682 objects detected in NGC 6334 IV. The continuous line marks the locus of the main-sequence stars (MS) taken from Koornneef (1983), while the two parallel dashed lines follow the standard reddening vectors (e.g. Tapia 1981) for late-and early-type stars. The cross indicates the typical photometric error

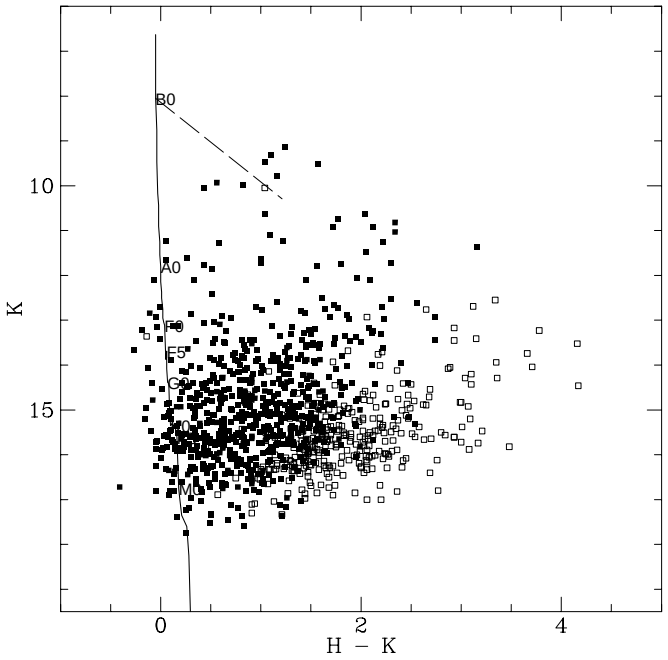

Fig. 4. K vs $H-K$ diagram of all the sources detected in the two colours towards NGC 6334 IV. The reddening vector corresponding to A_V=20 is indicated with a dashed line, while the continuous line is the locus of the main sequence stars at d=1.7 K pc. Filled squares are sources measured in JHK, and open squares are sources with only H and K measured

include each of the two large lobes of extended emission with highest apparent stellar density; c is an elongated section where the molecular cloud is densest and the known and suspected younger massive stellar objects are located and d is a section to the extreme SE of our survey area, believed to be dominated by field stars. These regions are indicated in Fig. 6, which shows a K band image of the area studied. For all the following statistical computations, the numbers have been normalized to the same unit area to facilitate comparisons.

In areas a and b (lobes), the number of stars (per sq arcmin) detected was 145 and 160, respectively, while areas d (reference) and c (dense cloud) had 84 and 95. The simplest possible explanations are that the actual density of stars is larger at zones a and b and/or that the interstellar extinction is much lower toward these zones than toward c and d. In the first case, given the observed characteristics of the molecular cloud, the hypothetical stellar cluster would have to be extremely young, similar to that in NGC 6334 I (Tapia et al. 1996). No evidence of this is found with our JHK photometry, quite the contrary.

In order to examine the second posibility, namely that there are significant differences in the average extinction, we shall assume that all sources detected in our survey in zones a, b and d are field stars. We then plot the distribution of the observed number of stars per unit area as a function of K magnitude for the whole area of study and for regions a, b (Fig. 7) that also show a similar exponential increase toward fainter bins. As expected, for the whole area the number of stars increases exponentially until we reach the completeness limit at K, which in our case is around 16. This distribution is very well fitted by that expected for field stars in this direction of the sky (Jones et al. 1981), with an added (local) extinction of $\langle A_K \rangle = 3.35$ (dashed line in the bottom panel of Fig. 7) on top of that caused by dust following the normal Galactic distribution. This implies that the average local extinction in the whole area is $A_V \simeq 31$. When applied to the observed distribution of stars in the lobes, the best fit is obtained for an added extinction of only $(A_K)_{\rm sl} = 2.5$ and $(A_K)_{\rm nl} = 2.2$ for the southern and northern lobes, respectively. This means that the average A_V in these regions is 23 in the south and 20 in the north. This method cannot be applied for regions c and d as the average extinction towards these zones is so high that the number of stars in the magnitude bins for $K < 16$ is too small to obtain a reliable fit.

An independent way of estimating the amount of extra interstellar extinction towards these regions is by computing the average value of the colour excess $E(H-K)$ in each direction. It has been demonstrated that for a complete survey of field stars performed at 2.2 μm the average intrinsic colour of the sample is $\langle (H-K)_0 \rangle = 0.11$ (Jones et al. 1981; Lada et al. 1994); we, thus, computed from our observed $(H-K)_{\rm obs}$ colour indexes, the average $\langle E(H-K) \rangle = \langle (H-K)_{\rm obs} - 0.11 \rangle$. The mean colour excesses turned out to be $\langle E(H-K) \rangle_{\rm sl} = 1.18$ and $\langle E(H-K) \rangle_{\rm nl} = 1.03$ yielding, for a standard reddening law (Rieke & Lebofsky 1982) $\langle A_V \rangle_{\rm sl} = 19$ and $\langle A_V \rangle_{\rm nl} = 15$. Clearly, if a significant fraction of the stars in the sample are early-type (ie. with bluer $(H-K)_0$), these values represent lower limits to $\langle A_V \rangle$. We note that there are 13 stars in the

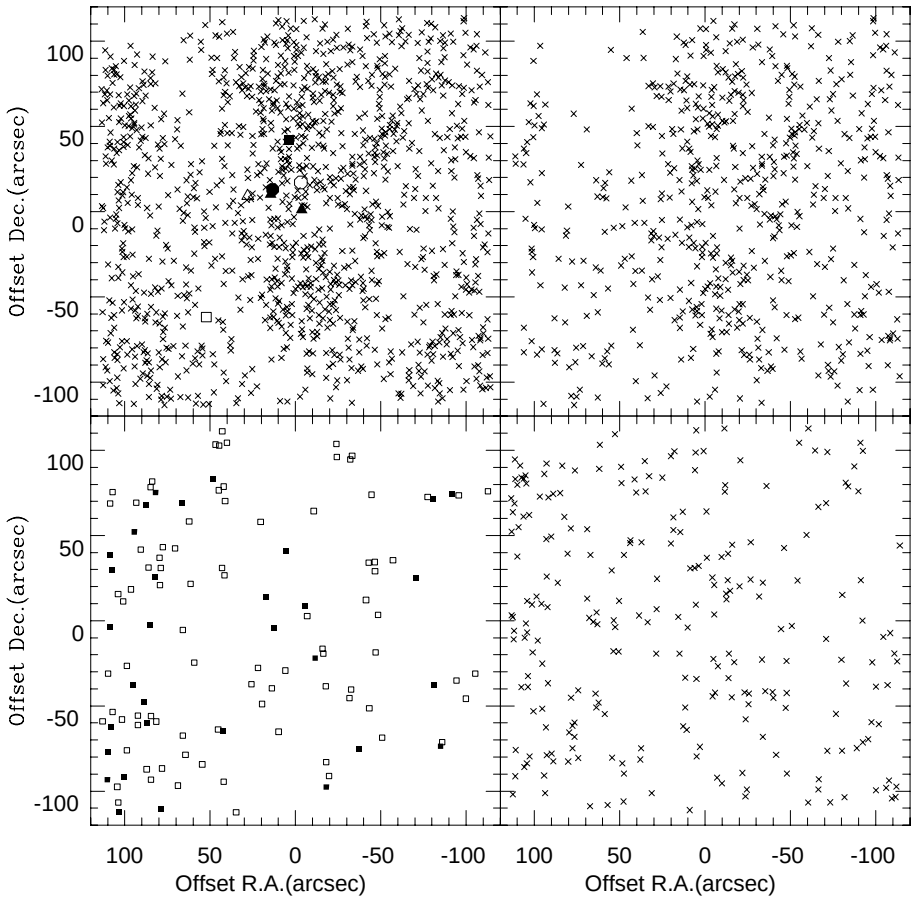

Fig. 5. Spatial distribution of the infrared sources detected in our survey. The position of the HII region (filled circle), of the H_2O maser (open circle), of the FIR peak (open triangle) and of the two 20 μm sources (filled triangles) are indicated. *Upper left panel:* all sources observed in K-band; *upper right panel:* sources with no infrared excess as deduced from the colour-colour plot; *lower left panel:* sources with IR excess (filled squares), and sources with $H-K$ $\geq$2.5 not detected in J; *lower right panel:* sources detected only in the K-band

southern lobe and 8 in the northern lobe with JHK colours corresponding to atmospheres of early (B0 to A) type stars that on average are reddened by $\langle A_V \rangle_{\rm sl} \simeq 25 \pm 2$ (sdm) and $\langle A_V \rangle_{\rm nl} \simeq 17 \pm 1$ (sdm) and are associated with these structures (see Sect. 3.5).

From molecular line radio observations and lower limits to the near-infrared emission of certain very young stellar objects, Kraemer et al. (1997) and Harvey et al. (1987) have established that the extinction toward the densest parts of the cloud (zone c) exceeds A_V = 100. On the other hand, Rodríguez et al. (1988) compared the 6 cm radio continuum flux from the ionized gas in the lobes with that measured by Harvey et al. (1987) for the diffuse emission at 2.2 μm from the same regions assuming that both arise from thermal free-free emission. They concluded that the mean extinction was $A_V = 17$ for the southern lobe a and $A_V = 11$ for the northern lobe b.

The lower mean values in the extinction measured towards the gas compared to those measured statistically toward the stars may be another indication that in the lobes the majority of the stellar population detected at 2 μm is in the *background*. Although a few stars in the northern and southern lobes may be associated with the molecular cloud, particularly those with JHK colours of reddened early-type stars or with excess emission at $\lambda > 2.0\,\mu$m, examination of the two-colour and magnitude-colour diagrams confirms the absense of a stellar population that resembles that of an embedded cluster in either of the two lobes. Thus, we conclude that there is no clear evidence of the presence of developed embedded clusters in these regions.

3.3. The central region

The central region of NGC 6334 IV, which we have labeled c, is characterized by the presence of a massive molecular disk detected by Kraemer et al. (1997), from which, according to these authors, NGC 6334 A, the water vapor maser and the young object HHS 20 have condensed, forming a *protocluster* of massive stars. This region was mapped at high resolution in the ammonia NH_3(3,3) line (Kraemer et al. 1997), in the mid-IR (Kraemer et al. 1999) and recently in the radio continuum (Jackson & Kraemer 1999) and at submillimeter and millimeter wavelengths (Sandell 1999). Fig. 9 of Kraemer et al. (1999) shows the correspondence of the five ammonia peaks with the other sources found in the region. Note that one of the ammonia clumps, is coincident with the H_2O maser.

Using our high spatial resolution near-IR images, we identify the near-IR sources associated with millimeter peaks, mid-IR sources and ammonia clumps. Table 2 lists coordinates and magnitudes of the relevant red objects found in the central area shown in Fig. 8, which shows our K-band image with the 1.1 mm continuum contours taken from Sandell (1999) overlaid. One of the main results from the analysis of this image is that the highly luminous object HHS 20 found by Harvey et al. (1987)

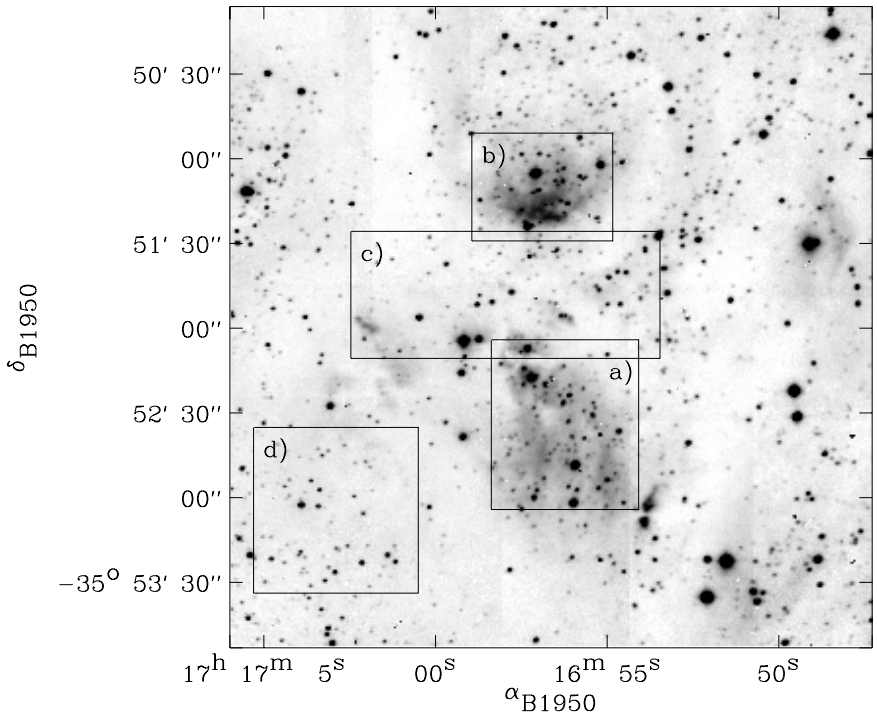

Fig. 6. K-band mosaic of NGC 6334 IV. The four rectangles delineate the areas used for the statistical study (see text)

is composed of three separate sources, labeled c1, c3 and c4 in Fig. 8. The infrared colours of c4 indicate that this is a field star. On the other hand, c1 and c3 are very red objects that coincide, respectively, with the mid-IR sources KDJ3 and KDJ3E of Kraemer et al. (1999). In particular, c1 is extended at 2.2 μm, as is also observed in the mid-IR, probably implying that at the shortest wavelengths, we are looking at the radiation from an embedded young star scattered by a dusty circumstellar envelope and whose thermal radiation dominates at $\lambda > 5\,\mu$m. The spectral energy distributions of c1 and c3 from the near-IR to the radio continuum are shown in Fig. 9a. Combining our photometry at 2.2 μm with the 20.6 μm flux densities, we derived the infrared spectral index $n = \mathrm{dlog}(\nu \mathrm{F}_\nu))/\mathrm{dlog}(\nu)$ obtaining $n = -3.6$ and $n = -2.9$ for c1 and c3, respectively. These values imply that the two sources are very young embedded stellar objects of approximately the same luminosity. The very steep spectrum observed agrees with the presence of the continuum millimeter source MM2 reported by Sandell (1999). Integrating the spectral energy distribution displayed in Fig. 9a, we derived a total luminosity of $\sim 2000 L_\odot$ for c1 and c3. Our estimated infrared luminosity agrees well with that of the exciting star (B1) required to power the radio continuum emission measured by Jackson & Kraemer (1999) coincident with this source. In conclusion, source HHS 20, previously believed to be a very massive young stellar object, is a system composed of at least two ZAMS B2-B3 stars. It should be pointed out that Harvey & Gatley (1983) estimated (their Table 5) a total luminosity of $8\ 10^4\ L_\odot$ for IRS 3 = HHS 20. This value was quoted in their paper without proper justification and, in view of the present results, must now be discarded.

Two near-IR sources, c6 and c7 (Fig. 8), have been detected within the boundaries of the radio HII region NGC 6334 A. The

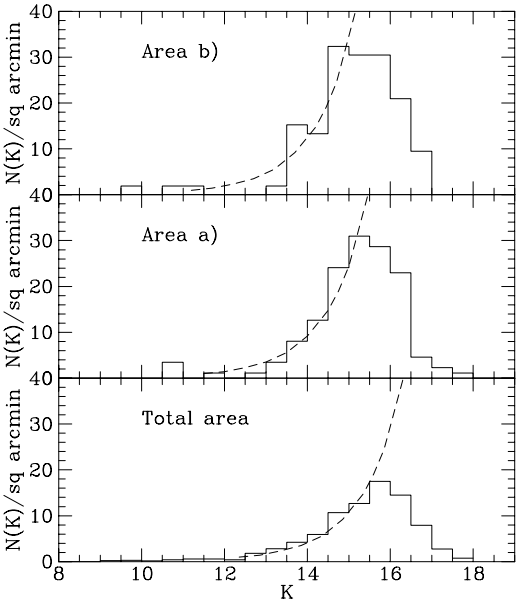

Fig. 7. Observed K-magnitude distribution for the total area surveyed, and for the two lobes a) and b). The dashed lines represent the distribution expected for field stars according to the model of Jones et al. (1981) for fitted values of additional *local* extinction (see text)

bright source c6 coinicides with the source HHS 19 of Harvey et al. (1987). Its near-IR colours are consistent with a reddened ($\mathrm{A}_V \sim 20$) early-type star with no excess at $\lambda < 2.5\,\mu$m, which is probably partially responsible for the excitation of the HII region. More interesting is the newly detected source c7 that shows a large near-IR excess. Its position, reported in Table 2, is very close to the 1.1 mm source MM1a of Sandell (1999).

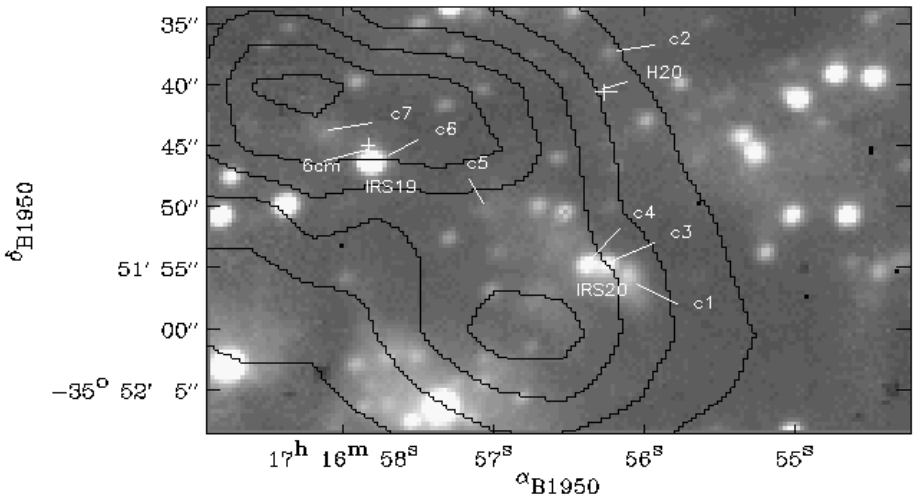

Fig. 8. K-band image of the central region with contours of the 1.1 mm emission (Sandell 1999) overlaid. The positions of the prominent near-IR sources are indicated, as listed in Table 2. The crosses mark the position of the H_2O maser (Rodríguez et al. 1980) and the centre of the radio HII region NGC 6334 A at 6 cm (Rodríguez et al. 1988)

Table 2. Prominent near-IR sources found in the central region of NGC 6334 IV

Irs	$\alpha(1950)$ h m s	$\delta(1950)$ ° ′ ″	K mag.	$H-K$	$J-H$	Identification.
c1	17 16 56.13	-35 51 55.4	14.54	2.69	$\geq$3.2	HHS20-IRS3, KDJ3, MM2
c2	17 16 56.26	-35 51 37.1	16.28			H_2O
c3	17 16 56.27	-35 51 54.4	14.13	$\geq$ 4.3		KDJ3E
c4	17 16 56.40	-35 51 54.4	13.91	0.77	1.05	
c5	17 16 57.00	-35 51 49.8	15.99			KDJ6
c6	17 16 57.84	-35 51 46.2	12.60	1.16	1.69	HHS19-IRS2, KDJ2
c7	17 16 58.13	-35 51 43.9	15.78	1.33	0.80	KDJ2, MM1a

The mid-IR source KDJ2 of Kraemer et al. (1999) was also resolved into two peaks at 12.5 μm and we associate them with the two sources, c6 and c7. Fig. 9b gives the infrared energy distribution of c6 and c7 obtained by combining the near-IR photometry with the millimeter, submillimeter and mid-IR flux densities. Integrating the spectral energy distribution, we evaluate an infrared luminosity for c6 and c7 of about 7500 $L_\odot$. Note that this luminosity corresponds to a cooler ZAMS than that required to power the radio HII region (Rodríguez et al. 1988), although this problem can be alleviated by the presence of other early B-type stars embedded in the central cloud. For a discussion on this discrepancy, see Jackson & Kraemer (1999).

Coinciding with the mid-IR source KDJ6 of Kraemer et al. (1999), we found another source (c5) detected only in K. Its spectral index $n = -3.6$ determined from the 2.2 and 20.6 μm flux densities suggests that this is another very young embedded object forming the protocluster together with the weak source (c2) detected only in K which lies approximately 3″ north of the H_2O maser and within one of the ammonia clumps. The position and photometry of the prominent sources found in the central area of NGC 6334 IV are given in Table 2.

3.4. The eastern region

A prominent (sub)millimeter source (MM3) was reported by Sandell (1999) approximately 75″ east of NGC 6334 A,. Within a few arcsec of its peak, we found very red (seen only at K) nebulous emission with a few localized maxima. We labeled these Irs1 to 8 on our K-band contour map (Fig. 10) and Table 3 lists their coordinates and magnitudes.

Table 3. List of the very red near-IR sources found in the area of the 1.1mm peak MM3.

Irs No.	$\alpha(1950)$ h m s	$\delta(1950)$ ° ′ ″	K mag.	$H-K$
1	17 17 01.11	-35 52 16.1	15.68	
2	17 17 01.58	-35 52 22.7	15.61	2.92
3	17 17 01.57	-35 52 07.5	15.80	2.08
4	17 17 01.92	-35 51 53.3	15.64	
5	17 17 01.88	-35 52 00.2	14.69	
6	17 17 02.08	-35 51 58.8	14.55	
7	17 17 02.12	-35 52 03.4	14.29	3.36
8	17 17 02.28	-35 51 56.4	14.64	

Following the analysis of the magnitude-colour diagram discussed by Tapia et al. (1996), we conclude that these sources cannot be background stars, but rather they are very young objects embedded in the cloud. The presence in emission of the CO 2–1 line found by Kraemer et al. (1997) and the (sub)millimeter peak imply that these sources and the IR nebula sorrounding them are signposts of yet another centre of active massive star formation in the 100–300 $M_\odot$ molecular clump that deserves further observations at all wavelengths as these regions were not covered by previous radio and mid-IR surveys.

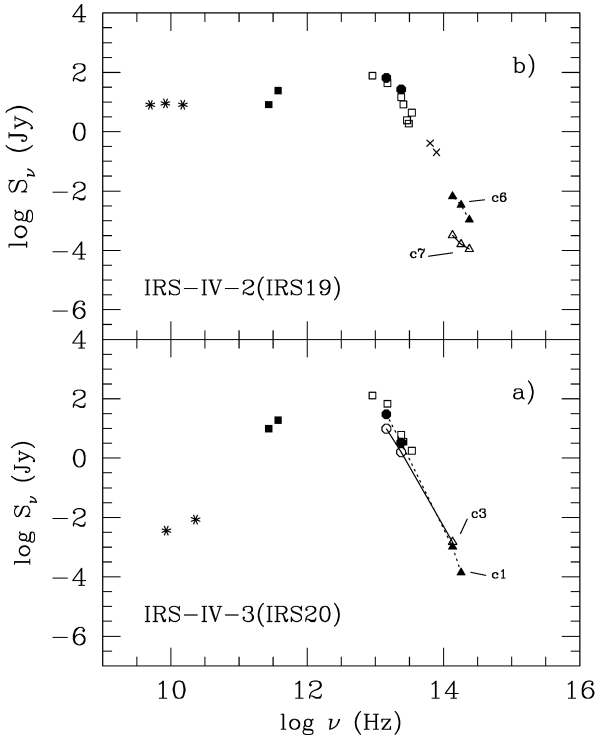

Fig. 9a and b. Spectral energy distribution of the sources in HHS20 **a** and HHS19 **b**. Data sources are: open squares from Harvey & Galtley (1983), asterisks from DePree et al. (1995) and Jackson & Kraemer (1999), filled squares from Sandell (1999), circles from Kraemer et al. (1999), crosses from Persi & Ferrari-Toniolo (1982) and triangles from this work

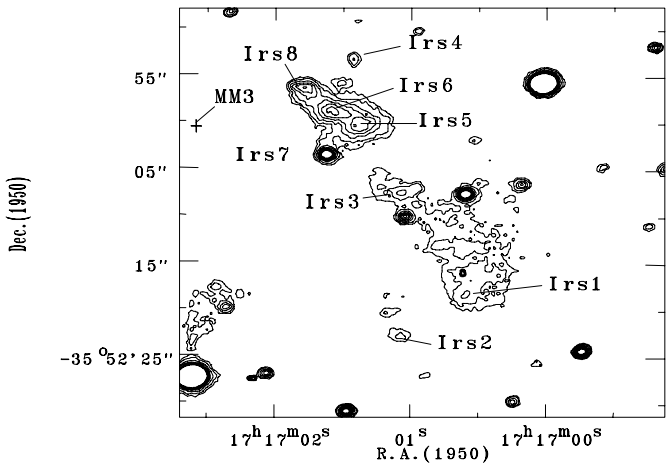

Fig. 10. K-band contour map of a region (44×44) sq arcsec in the vicinity of the (sub)millimeter peak MM3 (+; Sandell 1999). Sources are listed in Table 3. The contour levels are: (1.5, 2.2, 3.3, 4.3, 5.4, 7.6, 8.7, 9.8) $\times\ 10^{-5}$ Jy/beam. The beam is 2×2 pixels.

Finally, very close to the extended millimeter source MM4 of Sandell (1999) in the SE part of the region, we found a source (No. 13 in Table 1) with a significant near-IR excess, as well as a second very red object at $\alpha(1950) = 17^{\rm h}17^{\rm m}00.42^{\rm s}$ $\delta(1950) = -35^o53'01.9''$ with K=15.72, and $H-K$=3.00. These values also indicate that the star forming process has already started in this location.

3.5. Bipolar lobes and other conspicuous objects

The first evidence of gas emission in the neighbourhood of the far-infrared source NGC 6334 IV was found in the form of a very compact red nebulosity (GGD 25), resembling a Herbig-Haro object (Gyulbudaghian et al. 1978). The association of this object with the nearby HII region NGC 6334 A, the H_2O maser source and the far and mid-infrared objects as well as the nature of GGD 25 were unclear until Harvey & Gatley (1983) reported an extended 2.2 μm and 20 μm source coincident with the small optical nebula. Rodríguez et al. (1988) found very weak radio emission at the position of GGD 25 that seemed to be part of a more extended ionized gas emission. Bohigas (1992) demonstrated, through narrow-band imaging, that GGD 25 has optical line-emission properties of an HII region.

Even from the early 20 μm low resolution maps by Harvey & Gatley (1983), a bipolar morphology, centred on the mid-IR sources IRS2 and IRS3, was apparent. A follow-up work by Harvey et al. (1987) with higher resolution maps in the J, H and K bands showed the near-IR diffuse counterparts of the extended mid-infrared lobes to the north and south. Rodríguez et al. (1988) and DePree et al. (1995) presented further evidence that the two lobes are indeed physically associated with NGC 6334 A. First, the radio continuum maps show faint and diffuse emission connecting the northern and southern lobes with the central HII region and second, the radial velocities of the H92α emission from both lobes suggest an outflow phenomenon. Nevertheless, none of the maps in the wavelength range 2.2 to 20.6 μm show this "bridge" of emisssion in the central region.

The JHK images presented in this work, with the highest resolution to date, provide supplementary information to determine the nature of this emission. Fig. 11 shows contour plots of the diffuse 2.2, 1.6 and 1.2 μm, obtained by median-averaging (10×10) part of our original images. This procedure smoothed out all but the brightest stars. Note that the morphology is very similar in all three bands except that the emission tends to be fainter as the wavelength decreases. These JHK colours are reminiscent of free-free continuum, as suggested by Rodríguez et al. (1988).

Also marked in the K-band contour map is the position of the only bright Brγ spot determined by obtaining the continuum-subtracted image obtained with a filter containing this line. This corresponds to the position of GGD 25 and the 20.6 μm (Kraemer et al. 1999) and 14.8 μm (Kraemer & Jackson 1997) emission peaks, some arcsecs further north from the arc-like boundary of the northern lobe, remarkably well delineated at the shorter end of the thermal IR, from 3.6 to 6.8 μm (Kraemer & Jackson 1997; Jackson et al. 1999).

We propose the following scenario to explain the emission characteristics and morphology of the northern and southern lobes: The radio and near-infrared emission of the lobes arise from free-free emission from gas ionized mostly, but not solely,

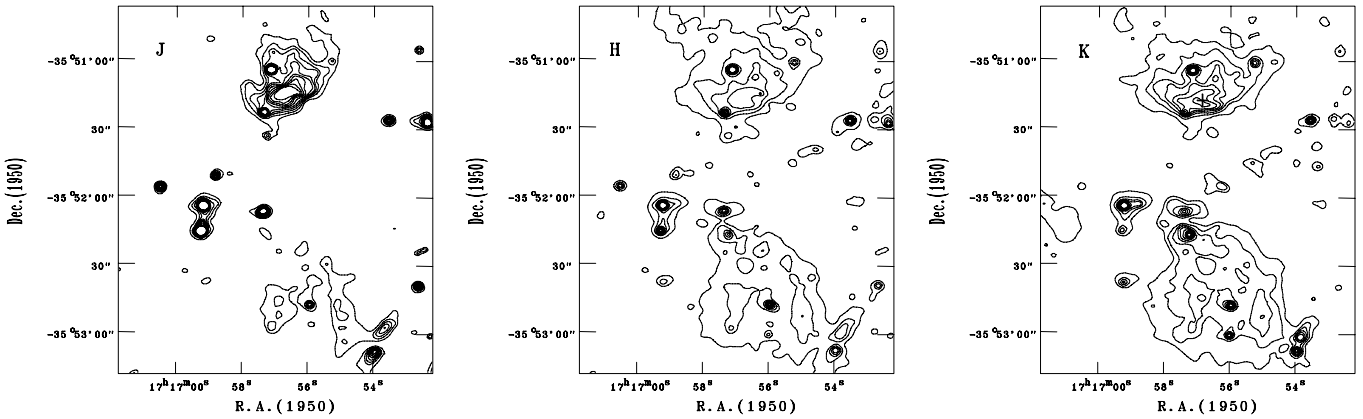

Fig. 11. Median-filtered (10×10) JHK-contour maps of the central region of NGC 6334 IV with most stars smoothed out. The Brγ spot at the position of GGD25 is indicated with the plus sign in the K-band panel. The contours start at 1.3 10^{-5} Jy/beam in K, 2.6 10^{-5} Jy/beam in H, 1.0 10^{-5} Jy/beam in J, and are spaced by the same fluxes per beam.

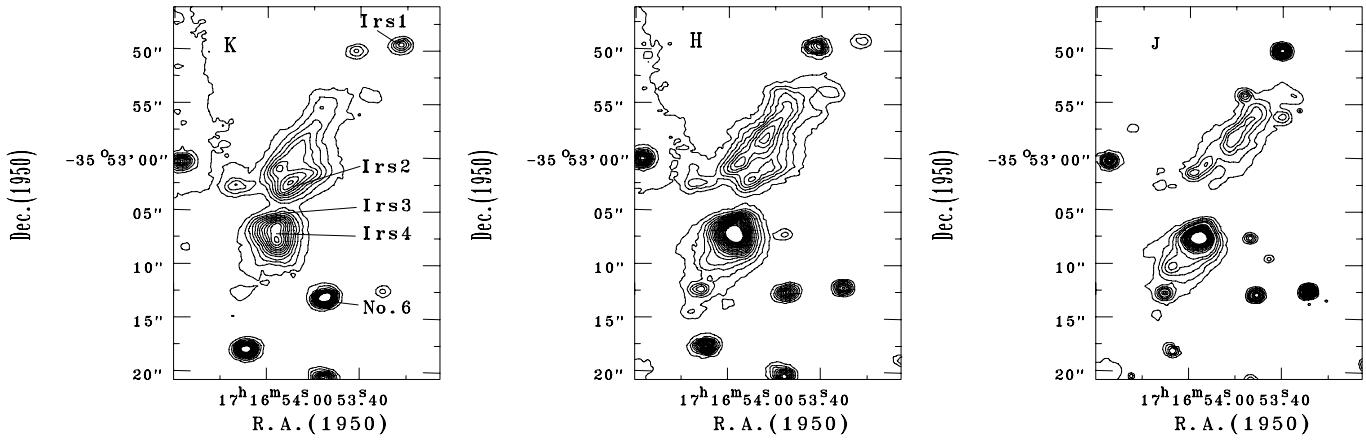

Fig. 12. JHK contour plots (2×2 pixel beam) of the SW bipolar nebula. The contours start at 2.8 10^{-5} Jy/beam in K, 3.6 10^{-5} in H, 2.9 10^{-5} Jy/beam in J, and are spaced by the same fluxes per beam.

by the central embedded luminous young objects IRS 2 and IRS 3, whose UV radiation passes through the north and south holes of the toroid. A number of other stars (see Sect. 3.1) associated with NGC 6334 IV in both lobes contribute to ionize the gas in the lobes and, particularly near the hot spots marked by the 14.8 and 20.6 μm peaks, increase the dust temperature, thus enhancing its thermal emission. As concluded in Sect. 3.2 and also pointed out by Rodríguez et al. (1988) and Harvey et al. (1987), the lower mean extinction of the northern lobe permits a small part of the HII region to shine at visible wavelengths (GGD 25). Therefore this giant bipolar structure (0.7 pc in size) was created by massive stellar winds collimated by the action of the dense toroid in the central region (cf. DePree et al. 1995)

Another interesting object with a small-scale bipolar morphology is observed in the SW part of our surveyed region. As shown in Fig. 1 and Fig. 11, it is located at the SW edge of the southern radio lobe, in a region which had been left out of previous radio and mid-infrared surveys (Rodríguez et al. 1988, Jackson & Kraemer 1999, Kraemer et al. 1999). This bipolar object has a major axis of aproximately 25″or 0.2 pc (at $d = 1.7$ kpc). Fig. 12 displays the J, H and K contour plots of this object. Extended nebular emission from both the northern and southern poles is present at all wavelengths with a thick dust lane separating them. As seen in other young bipolar structures, the thickness of this lane increases with decreasing wavelength, confirming the nature of the dust extinction. The presence of an edge-on thick toroid is thus inferred. Two very red sources, labelled Irs2 and Irs3 in Fig. 12, are located in the innermost part (closest to the toroid) of each lobe. Their magnitudes and colours (Irs2: $K = 13.68$, $H - K = 1.87$; Irs3 $K = 13.58$, $H - K \geq 2$) indicate (cf. Fig. 4) that, if confirmed as individual stars, these are of a late-B type with $A_V \geq 20$. Alternatively, it may be that both Irs2 and Irs3 are just knots of reflection of the light of a hidden more luminous star at the centre of the toroid and until longer wavelength observations are avaliable, no further conclusions can be made, particularly as Irs3 is too close to a bright star with JHK colours corresponding to a reddened late-type (presumably field) star. Two other sources present in the area show significant near IR excesses. Object 6 is reported in Table 1, while Irs1 with $K = 14.65$ and $H - K = 2.02$

could be another late-B type star associated with the cloud. The diffuse emission appears to be light from the embedded objects scattered by the dust cloud.

4. Conclusions

From the analysis of our sub-arc-resolution and very deep near-IR images of the active centre of massive star formation NGC 6334 IV and of the colour-colour and colour-magnitude we can derive the following conclusions:

1) Of the 682 sources with measured JHK colours, only 32 sources were found to exhibit near-IR excess. These sources are distributed in an area of size 230×230 sq arcsec centred on the shell-shaped HII region NGC 6334 A. No evidence of a massive developed young stellar cluster of the type found in NGC 6334 I and NGC 3576 (Tapia et al. 1996; Persi et al. 1994) has been found.

2) In the densest part of NGC 6334 IV (the central region) where a *protocluster* of massive stars is being formed, we identified near-IR counterparts of the mid-IR sources reported by Kraemer et al. (1999). In particular, source HHS20, believed to be a very massive young stellar object, is found to be a system composed of at least two ZAMS B2–B3 stars. HHS19 was also found to be multiple and the presence of other luminous embedded young stellar objects was also discovered in this region.

3) Analysis of the morphology of the giant bipolar lobes in the radio and in the near and mid-IR indicates that the giant bipolar structure is created by massive stellar winds collimated by the action of the dense toroid in the central region. In the lobes, gas thermal (free-free) emission dominates in the near-IR and radio, while heated dust, well-mixed with the gas, is responsable for the mid-IR emission. We confirm that the extinction is higher toward the southern lobe than toward the northen one but both are less reddened than their immediate surroundings.

4) A new massive centre of star formation is found to the east of the central region, where an IR nebula and several very red point-like near-IR sources are also present. These lie close to a (sub)millimeter peak and to where emission of the CO(2-1) line has also been reported..

5) The only low luminosity young stellar object in our survey is a small ($25''$) bipolar nebula located close to the SW edge of the giant southern lobe and several nearby stellar objects with large near-infrared excess.

Acknowledgements. We acknowledge partial support from Conacyt (Mexico)-CNR(Italy) binational program. MT was supported by DGAPA-UNAM grant IN108696

References

Bohigas J., 1992, Rev. Mex. Astr. Astrofis. 24, 121
DePree C.G., Rodríguez L.F., Dickel H.R., Goss N.M., 1995, ApJ 447, 220
Dickel H.R., Dickel J.R, Wilson W.J., 1977 ApJ 217, 56
Emerson J.P., Jennings R.E., Moorwood A.F.M., 1973, ApJ 184, 401
Gyulbudaghian A.L., Glushkov Yu. J., Denisyuk E.K., 1978, ApJ 224, L137
Harvey P.M., Gatley I., 1983, ApJ 269, 613
Harvey P.M., Hyland A.R., Straw S.M., 1987, ApJ 317, 173
Jackson J.M., Kraemer K.E., 1999, ApJ 512, 260
Jackson J.M., Kraemer K.E., Gatley I., et al., 1999, BAAS 194, 1111
Jones T.J., Ashly M., Hyland A.R., Ruelas-Mayorga A., 1981, MNRAS 197, 413
Koornneef J., 1983, A&A 128, 84
Kraemer K.E., Jackson J.M., 1997, BAAS 29, 1217
Kraemer K.E., Jackson J.M., Paglione T.A., Bolatto A.D., 1997, ApJ 478, 614
Kraemer K.E., Deutsch L.K., Jackson J.M., et al., 1999, ApJ 516, 817
Lada C.J., Lada E.A., 1991, ASP Conf. Ser. vol.13, p. 3
Lada C., Lada E.A., Clemens D.P., Bally J., 1994, ApJ 429, 694
Loughram L., McBreen B., Fazio G.G., et al., 1986, ApJ 303, 629
McBreen B., Fazio G.G., Stier M., Wright E.L., 1979, ApJ 232, L183
Neckel T., 1978, A&A 69, 51
Persi P., Ferrari-Toniolo M., 1982, A&A 112, 292
Persi P., Roth M., Tapia M., et al., 1994, A&A 282, 474
Persi P., Roth M., Tapia M., et al., 1996, A&A 307, 591
Persson S.E., West S.C., Carre D.M., et al., 1992 PASP 104, 204
Rieke G.H., Lebofsky M.J., 1985, ApJ 288, 618
Rodríguez L.F., Moran J.M., Ho P.T.P., Gottlieb E.W., 1980, ApJ 235, 845
Rodríguez L.F., Cantó J., Moran J.M., 1982, ApJ 225, 103
Rodríguez L.F., Cantó J., Moran J.M., 1988, ApJ 333, 801
Sandell G., 1999, A&A 343, 281
Stetson P.B., 1987, PASP 99, 191
Straw S.M., Hyland A.R., McGregor P.J., 1989, ApJS 69, 99
Tapia M., 1981, MNRAS 197, 949
Tapia M., Roth M., Lopez J.A., et al., 1991, A&A 242, 388
Tapia M., Persi P., Roth M., 1996, A&A 316, 102
Tapia M., Persi P., Bohigas J., Ferrari-Toniolo M., 1997, AJ 113, 1769